

Citrate-Based Tannin-Bridged Bone Composites for Lumbar Fusion

Jinshan Guo, Xinggui Tian, Denghui Xie, Kevin Rahn, Ethan Gerhard, Michelle Laurel Kuzma, Dongfang Zhou, Cheng Dong, Xiaochun Bai,* Zhihui Lu,* and Jian Yang*

Conventional bone composites consistently fail to mimic the chemical composition and integrated organic/inorganic structure of natural bone, lacking sufficient mechanics as well as inherent osteoconductivity and osteoinductivity. Through a facile surface coating process, the strong adhesive, tannic acid (TA), is adhered to the surface of the natural bone component, hydroxyapatite (HA), with and without the immobilization of *in situ* formed silver nanoparticles. Residual functional groups available on the immobilized TA substituents are subsequently covalently linked to the citrate-based biodegradable polymer, poly(octamethylene citrate) (POC), effectively bridging the organic and inorganic phases. Due to the synergistic effects of the tannin and citrate components, the obtained citrate-based tannin-bridged bone composites (CTBCs) exhibit vastly improved compression strengths up to 323.0 ± 21.3 MPa compared to 229.9 ± 15.6 MPa for POC-HA, and possess tunable degradation profiles, enhanced biomineralization performance, favorable biocompatibility, increased cell adhesion and proliferation, as well as considerable antimicrobial activity. *In vivo* study of porous CTBCs using a lumbar fusion model further confirms CTBCs' osteoconductivity and osteoinductivity, promoting bone regeneration. CTBCs possess great potential for bone regeneration applications while the immobilized TA additionally preserves surface bioconjugation sites to further tailor the bioactivity of CTBCs.

1. Introduction

Bone serves as the body's support structure and mineral reservoir, protecting vital organs, producing hematopoietic derived cells, and helping maintain acid-base homeostasis in the body.^[1–3] With ≈ 1.6 million procedures being performed annually in the United States alone, bone transplantation is one of the most common tissue transplant procedures.^[4] Although autograft bone remains the gold standard for bone transplantation, the quality and quantity of autografts are greatly limited. Furthermore, the use of autografts necessitates additional surgery, extended recovery time and increased risk of postoperative complications.^[5–7] Thus, the development of fully synthetic and biomimetic bone substitutes that restore the function of natural bone is in high demand.

To mimic the structure of natural bone, which is composed of 60–65 wt% hydroxyapatite (HA, inorganic) embedded in a collagen (organic) matrix,^[5,6,8] extensive research effort has been made to develop

Prof. J. Guo, X. Tian, Prof. D. Xie, Prof. D. Zhou, Prof. X. Bai, Prof. Z. Lu

Department of Histology and Embryology
School of Basic Medical Sciences
Department of Orthopedic Surgery
The Third Affiliated Hospital of Southern Medical University
Southern Medical University
Guangzhou 510515, P. R. China
E-mail: baixc15@smu.edu.cn; luzhihui107@sohu.com

Prof. J. Guo, X. Tian, Prof. D. Xie, Prof. D. Zhou, Prof. X. Bai, Prof. Z. Lu

Academy of Orthopedics of Guangdong Province
Guangdong Provincial Key Laboratory of Bone and Joint Degeneration Diseases
Guangzhou 510630, P. R. China

Dr. J. Guo, K. Rahn, E. Gerhard, Dr. M. L. Kuzma, Prof. C. Dong, Prof. J. Yang

Department of Biomedical Engineering
Materials Research Institute
The Huck Institutes of The Life Sciences
The Pennsylvania State University
University Park, PA 16802, USA
E-mail: jxy30@psu.edu

X. Tian
Department of Spine Surgery
The Affiliated Hospital of Southwest Medical University
Luzhou, Sichuan 646000, P. R. China

Prof. D. Zhou
School of Pharmaceutical Sciences
Southern Medical University
Guangzhou 510515, P. R. China

Prof. X. Bai
Department of Biology
School of Basic Medical Sciences
Southern Medical University
Guangzhou 510515, P. R. China

 The ORCID identification number(s) for the author(s) of this article can be found under <https://doi.org/10.1002/adfm.202002438>.

DOI: 10.1002/adfm.202002438

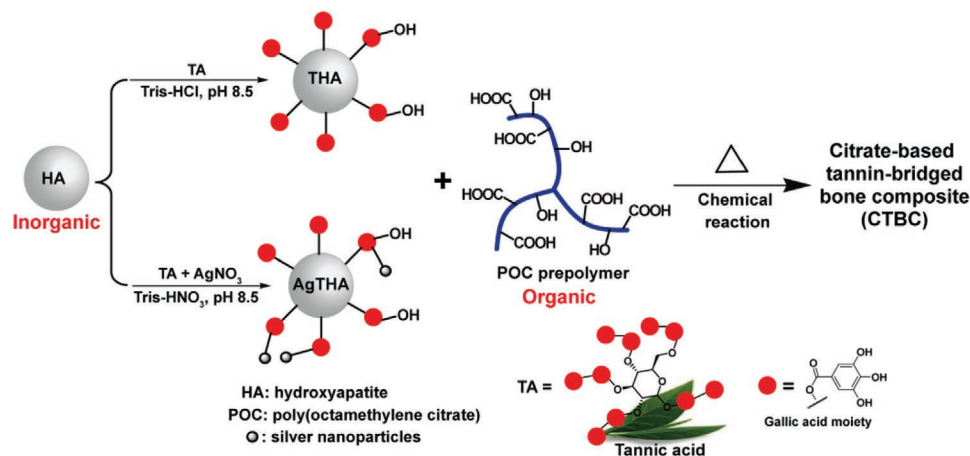
organic/inorganic bone composites as bone substitutes.^[5,6,8,9] Calcium phosphates (CaPs), such as HA and β -tricalcium phosphate (β -TCP),^[5,6,9–11] and bioactive glasses,^[12] are often used to approximate the inorganic components of bone. Organic polymers used in bone composites include biologically derived and biodegradable polymers, such as collagen,^[13] gelatin,^[14,15] chitosan,^[16] poly(lactic acid) (PLA), poly(glycolic acid) (PGA), poly(ϵ -caprolactone) (PCL) and their respective copolymers.^[10,11] Although promising, the compatibility of the organic and inorganic components is often far from ideal, leading to inorganic/organic phase separation, reduced mechanical properties, and failed bone integration and regeneration.^[5,6,9] To address these problems, HA has been surface modified with L-lactic acid (LA) oligomers,^[10,11] poly(amino acid)^[17] or poly(N-isopropylacrylamide) (PNIPAM).^[18] After surface “organic” modification, the organic/inorganic composites exhibited enhanced mechanical properties, uniform microstructures and prolonged mechanical durability during degradation.^[11] However, these surface modification strategies are greatly limited by the surface properties of inorganic particles,^[11] often making pre-treatment of the inorganic surface necessary to provide immobilized initiating sites.^[17,18] A universal strategy to bridge inorganic particles and organic polymers is urgently needed.

Marine creatures, such as the blue mussel, can strongly adhere to a range of nonspecific surfaces under water via excreted proteinaceous fibers presenting catechol moiety L-DOPA (L-3,4-dihydroxyphenylalanine). Inspired by nature, in recent years the science community has achieved remarkable successes utilizing mussel-inspired and similar tannin-inspired adhesion strategies in tissue adhesive development,^[9,19–24] materials engineering and surface functionalization.^[25–29] The catechol or gallotannin (tannin) species employed by these strategies not only strongly adhere to biological surfaces through the formation of covalent bonds under oxidizing conditions, but also strongly adhere to inorganic and metallic surfaces via surface bonding, hydrogen bonding or the formation of catechol/gallol-metal complexes.^[21,30] This versatile bonding capability renders catechol and tannin species ideal “bridging” molecules between inorganic and organic phases. Mussel-inspired dopamine and polydopamine, tannin, and

other polyphenols have been used to modify or coat inorganic and metallic surfaces to enhance cell adhesion,^[11,29,31] HA crystallization and biomineralization,^[32,33] and osteogenic effects relative to bare counterparts.^[34,35] Moreover, polyphenols can confer antioxidant,^[29,36] antimicrobial,^[24,29,37] and hemostatic features as well as the ability to promote migration of stem cells and accelerate wound healing.^[38] Finally, due to their distinctive chemical structure and high functional group density, surface immobilized tannin molecules preserve a multitude of functionalities, which can be used for further modification or to chemically react with compositing organic polymers, a potent feature never fully exploited.

Ideal compositing organic polymers for orthopedic tissue engineering should not only be biodegradable, but also bioactive, exhibiting osteoconductivity and osteoinductivity. Yang Lab has focused on the development of citrate-based biomaterials, which have demonstrated marked potential in orthopedic applications due to the versatile citrate chemistry platform in addition to the chemical and biological benefits of citrate in osteogenesis.^[5,6,9,39–41] As a key intermediate of the Krebs cycle, citrate is highly concentrated in native bone, with 90% of the body’s total citrate located in the skeletal system.^[42] Citrate is a critical bioactive factor in bone, having roles in calcium dissolution as well as apatite nanocrystal structuring during natural bone formation.^[42,43] Furthermore, “osteoblast citration” (the role of osteoblasts as specialized citrate producing cells that provide the source of citrate in bone formation) has also been found to be crucial in osteogenic differentiation and mineralization.^[39] Recent findings from Yang Lab have elucidated mechanisms supporting the promotion of osteogenic differentiation of human mesenchymal stem cells (hMSCs) upon exposure to exogenous citrate. It was found that metabolic pathways facilitate increased uptake of extracellular citrate during osteogenic differentiation through a process referred to as metabonegenic regulation to accommodate the initial high metabolic activity necessary for hMSC differentiation.^[44]

In this work, tannic acid (TA) was coated on the surface of HA particles through a facile one-step reaction to yield HA modified with TA (THA) (Scheme 1). In situ forming silver



Scheme 1. The synthesis of tannic acid modified hydroxyapatite (THA) and of silver nanoparticle and tannic acid modified hydroxyapatite (AgTHA) followed by subsequent reaction with poly(octamethylene citrate) (POC) prepolymer yielding citrate-based and tannin-bridged bone composites (CTBCs).

nanoparticles (Ag NPs) can also be immobilized onto the surface of HA during the one-step reaction process to produce HA modified with TA and silver (AgTHA) in order to confer antimicrobial activity (Scheme 1). Both THA and AgTHA preserve unreacted hydroxyl groups on immobilized TA molecules which were chemically reacted with the carboxylic acid groups available in the prepolymer of the citrate-based biodegradable polymer, poly(octamethylene citrate) (POC),^[40,45] creating a stable tannin bridged inorganic/organic matrix. The efficiency of this strategy to enhance the compatibility between inorganic (HA) and organic (POC) phases was investigated. The mechanical properties, degradation profiles, biomineralization performance, biocompatibility and antibacterial capability were studied *in vitro*. Furthermore, *in vivo* study of porous POC-HA, POC-THA, POC-HA/THA and POC-THA/AgTHA composite scaffolds was conducted using a lumbar fusion model in rabbits to further evaluate the bone regeneration performance of citrate-based tannin-bridged bone composites (CTBCs).

2. Results and Discussion

2.1. HA Modification

In traditional HA surface modification strategies, most of the coupling agents including organic isocyanates,^[46] LA oligomers,^[10,11] silane coupling agents,^[17,18] and polyacids^[47] are grafted onto HA surfaces through covalent bonding with surface hydroxyl groups. However, both the amount and the reactivity of the active hydroxyl groups on the HA surface are limited, greatly hindering the application of these strategies. In contrast, mussel-inspired and tannin-inspired surface coating strategies are universally applicable to nonspecific surfaces, such as underwater rock, inorganic microparticles, or polymeric microspheres, regardless of surface properties.

After a facile one-step reaction, two peaks at 1750–1550 cm^{-1} appeared in the FTIR spectra of THA and AgTHA (Figure 1A) which were not found in the FTIR spectrum of HA and can be assigned to the characteristic absorbance of the ester bonds in

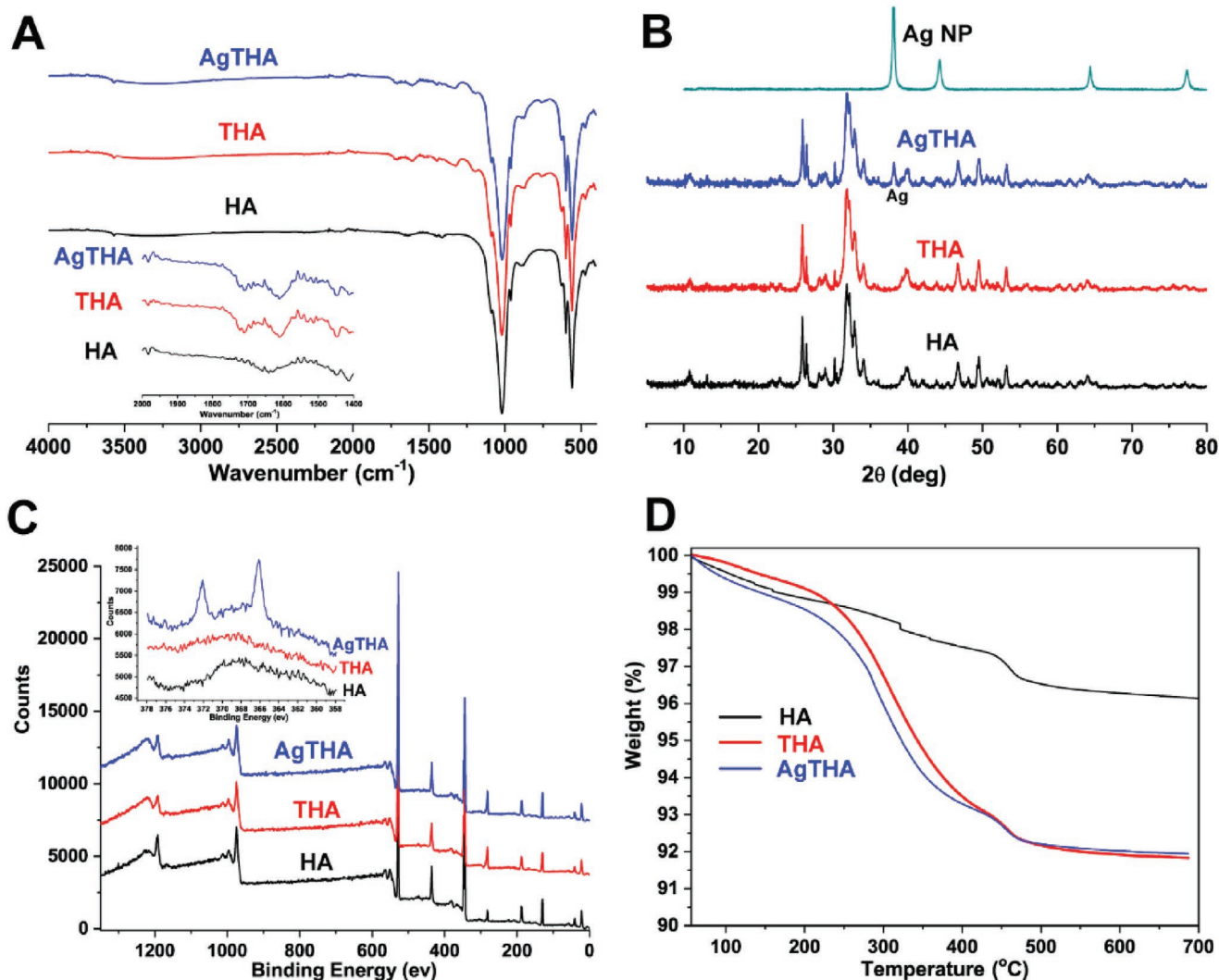


Figure 1. A) FTIR, B) XRD, and C) XPS spectra, as well as D) TGA curves of HA, THA, and AgTHA. Characteristic peaks are inserted as enlarged spectra in (A) and (C) for the comparison of different samples.

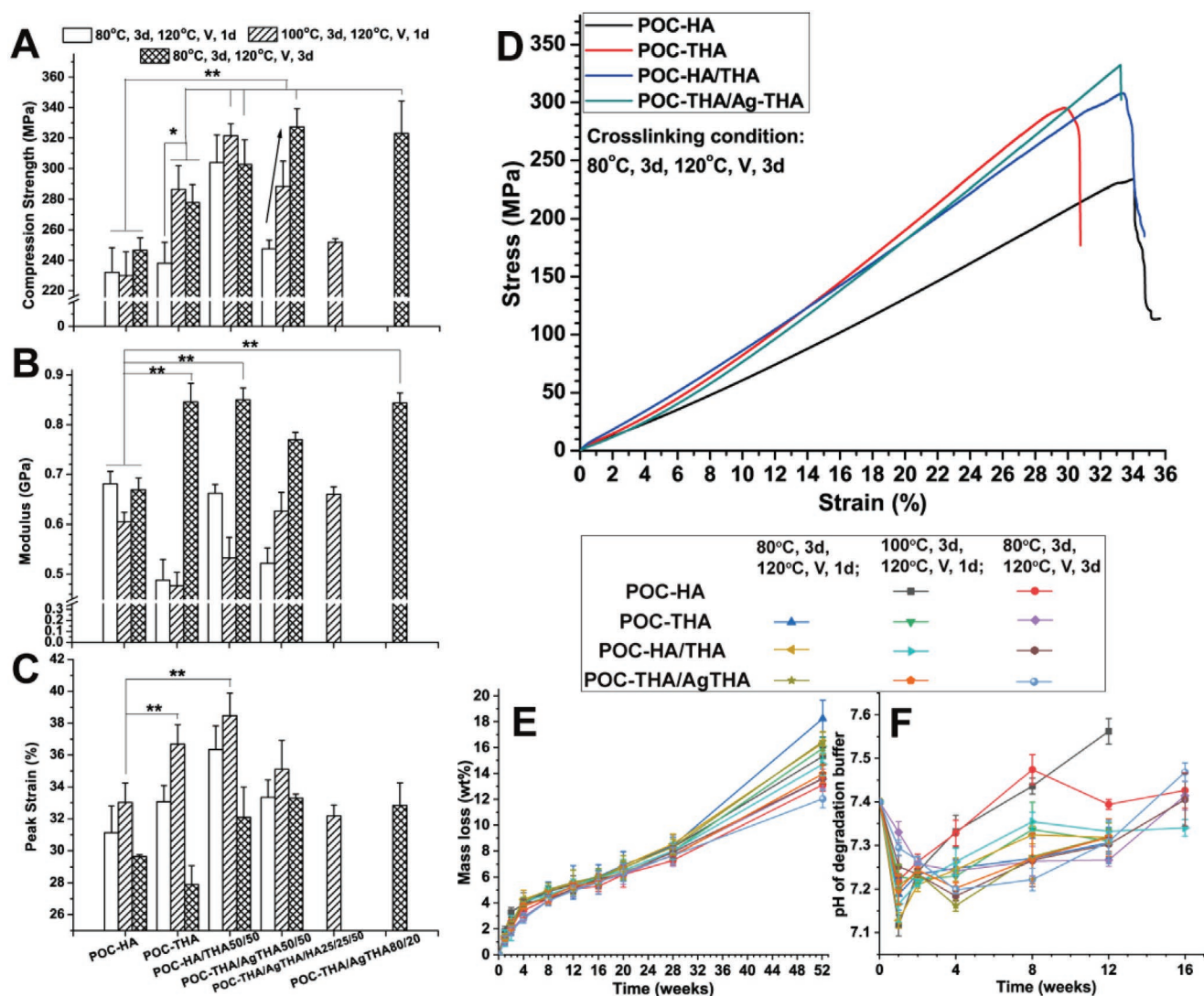


Figure 2. A) Compression strengths, B) moduli, C) peak strains, and D) representative stress-strain curves of POC-HA, POC-THA, POC-HA/THA 50/50, POC-THA/AgTHA 50/50, POC-THA/AgTHA/HA 25/25/50, and POC-THA/AgTHA 80/20 crosslinked at different conditions. E) Degradation profiles and F) change in pH of the degradation buffer of POC-HA, POC-THA, POC-HA/THA (50/50), POC-THA/AgTHA (50/50) composites in PBS (pH 7.4) at 37 °C. * $p < 0.05$, ** $p < 0.01$.

TA molecules. The characteristic peaks (38.1° , 44.2° , 64.4° , and 77.3°) of silver nanoparticles (Ag NPs) presented in the X-ray diffraction (XRD) spectrum of AgTHA (Figure 1B), confirming the successful immobilization of Ag NP on the surface of the modified HA. There is nearly no difference detected from the XRD spectra of HA and THA, implying that the surface modification of HA with TA had no influence on the crystal structure of HA (Figure 2B). The presence of Ag $3d_{3/2}$ and Ag $3d_{5/2}$ peaks at ≈ 373 and ≈ 366 eV, respectively,^[48] in the X-ray photoelectron spectroscopy (XPS) spectrum of AgTHA further confirmed the successful immobilization of Ag NPs onto HA (Figure 1C). The presence of carbon in THA and AgTHA as well as the presence of Ag in AgTHA samples detected through energy dispersive spectroscopy (EDS) analysis further supported the success of surface conjugation (Table S1). During thermogravimetric analysis (TGA) testing ($25\text{--}700^\circ\text{C}$, N_2 , $10^\circ\text{C min}^{-1}$), the differences of the weight loss percentages of HA (3.5% weight loss), THA

and AgTHA (both $\approx 8\%$ weight loss) indicated that $\approx 4.7\%$ wt% of TA was successfully coated onto THA and AgTHA (Figure 1D). Although the modification is conducted in a heterogeneous manner, if the reaction pH is controlled and vigorous stirring is applied, the modification process is controllable and repeatable.

2.2. Mechanical Properties and Degradation Profiles of POC-HA and CTBC Composites

Mechanical studies of POC-THA, POC-HA/THA, and POC-THA/AgTHA composite cylinders thermally crosslinked at different conditions were conducted with POC-HA as control. For all groups, mechanical strength increased with longer crosslinking time, higher temperature and vacuum application (Figure 2A–D). Regardless of crosslinking conditions, the compression strengths of POC-HA cylinders were lower than

250 MPa (Figure 2A). In contrast, the compression strengths of the composite cylinders containing THA, AgTHA or a mixture of the two were significantly higher, exhibiting strengths between 240–290 MPa for the POC-THA cylinders and up to 325 MPa for the POC-HA/THA and POC-THA/AgTHA cylinders (150–230 MPa for native bone) (Figure 2A). To explore whether HA modification with TA is a key to improve the mechanical properties of composite materials, POC/TA polymers were first synthesized by mixing POC prepolymer and TA followed by thermal crosslinking and characterization of their mechanical properties. The results show that the moduli of POC/TA films (w/w = 90/10, 85/15, and 80/20) all increased with the increase of TA contents. The tensile strengths and elongations also increased with the increase of TA for POC/TA_{90/10} and POC/TA_{85/15}. The above data suggests that the addition of polyfunctional TA in POC increased the crosslinking degree. However, the chemical reaction between POC prepolymer and TA consumed the carboxyl groups on POC prepolymer, thus attenuated the HA binding capability of POC. So when POC, TA and HA were mechanically mixed and crosslinked, although the moduli of POC/TA-HA cylinders increased with the increase of TA contents, the peak strains greatly reduced, leading to decreased compression strengths for all tested POC/TA-HA formula comparing to that of the POC-HA control (Figures S1D–F, Supporting Information). These results indicate that TA immobilization onto HA indeed played a critical role in bridging inorganic HA and organic POC to enhance the mechanical strength. The moduli and peak strains of the composite cylinders containing THA and/or AgTHA are shown in Figure 2B,C. A favorable balance between modulus and elongation is necessary to achieve a high compression strength (Figure 2A–C; Figure S1, Supporting Information), which is also reflected in the representative stress-strain curves shown in Figure 2D.

The degradation profiles of the crosslinked composite disks are shown in Figure 2E,F. Overall, the degradation rates of the composite disks in PBS (pH 7.4) were very slow with 10–20 wt% being degraded in one year (Figure 2E). This slow rate might be attributed to the strong complex between the hydroxyl groups on the surface of HA and modified HA with the carboxyl groups that are abundant in POC. The degradation rates of composite disks containing THA or AgTHA were faster than that of the POC-HA samples (Figure 2E). The pH values of the buffer solutions sampled when changing PBS after degradation were also monitored (Figure 2F). After a drop in the pH during the first week of degradation, the pH of the buffer solution quickly increased to and stabilized at a pH between 7.3–7.5, implying pH compatibility with surrounding tissues if the composite scaffolds were implanted in vivo.

2.3. TA Coating Promotes Biomineralization

To investigate the effects of TA coating on mineralization, in vitro mineralization of both modified HA particles and their composites with POC was conducted using HA and POC-HA as controls, respectively. As shown in Figure S2 in the Supporting Information, after one day of incubation, newly formed mineral crystal layers were observed. The thickness and density of

respective mineral crystal layers increased with incubation time. Although no substantial difference in mineralization capability was detected for THA, AgTHA and HA particles (Figure S2, Supporting Information), the effect of the TA coating was reflected in the results of the mineralization study of different composite disks (Figure 3). After incubation for one and seven days, more mineral deposition was observed on the CTBC composite disks than on POC-HA disks (Figure 3 insets), which can also be deduced from the change in densities and crystal sizes shown in the SEM images (Figure 3). These results agree well with previous literature indicating that polydopamine or natural polyphenol coatings can promote HA crystallization or biomineralization.^[32,33]

2.4. In Vitro Biocompatibility

The cytocompatibility of the composites was estimated by the cytotoxicity study of the degradation products of the composites using MTT (methylthiazolyldiphenyl-tetrazolium bromide) assay against human mesenchymal stem cells (hMSCs) (Figure 4A). Although the cell viabilities of the 1× degradation products of the composites (~30%) were significantly lower than that of the degradation product of PLGA (52.8 ± 4.08%) at 1× dilution, the cell viabilities of the degradation products of these composites at 10× and 100× dilutions were higher than that of PLGA degradation products at the same dilutions (Figure 4A). Cytotoxicity of the CTBCs and POC-HA were similar (Figure 4A). The cell proliferation of hMSCs on composite films was also evaluated by the MTT assay and SEM imaging using commercially available tissue culture treated plates (Costar, USA) as control (Figure 4B,C). The cell numbers on the composite films containing THA and/or AgTHA were higher than on the POC-HA films as early as one day after seeding (Figure 4B) indicating better cell adhesion on the films containing TA. After the initial cell adhesion, hMSCs grew better on these composite films relative to the POC-HA films as indicated by higher cell counts 7 days post cell seeding on the composite films (Figure 4B) coinciding with the SEM images on day 7 (Figure 4C). These results suggest that the inclusion of TA and Ag NP did not induce significant cytotoxicity, and provide further evidence that the inclusion of a polyphenol or polydopamine compound can promote cell adhesion and proliferation as reported previously.^[11,29,31]

2.5. Antibacterial Performance

The antibacterial performance of THA and AgTHA particles (HA as control) as well as POC-THA, POC-HA/THA and POC-THA/AgTHA composites (POC-HA as control) was tested against *Staphylococcus aureus* (*S. aureus*) and *Escherichia coli* (*E. coli*) as representative Gram-positive and Gram-negative bacteria, respectively.

The minimal inhibitory concentrations with 100% bacterial inhibition (MICs) of HA, THA, and AgTHA particles were determined using the agar dilution method.^[22–24] As shown in Figure 5A,B and Figure S2 (Supporting Information), unmodified HA had nearly no antibacterial effect against *S. aureus*

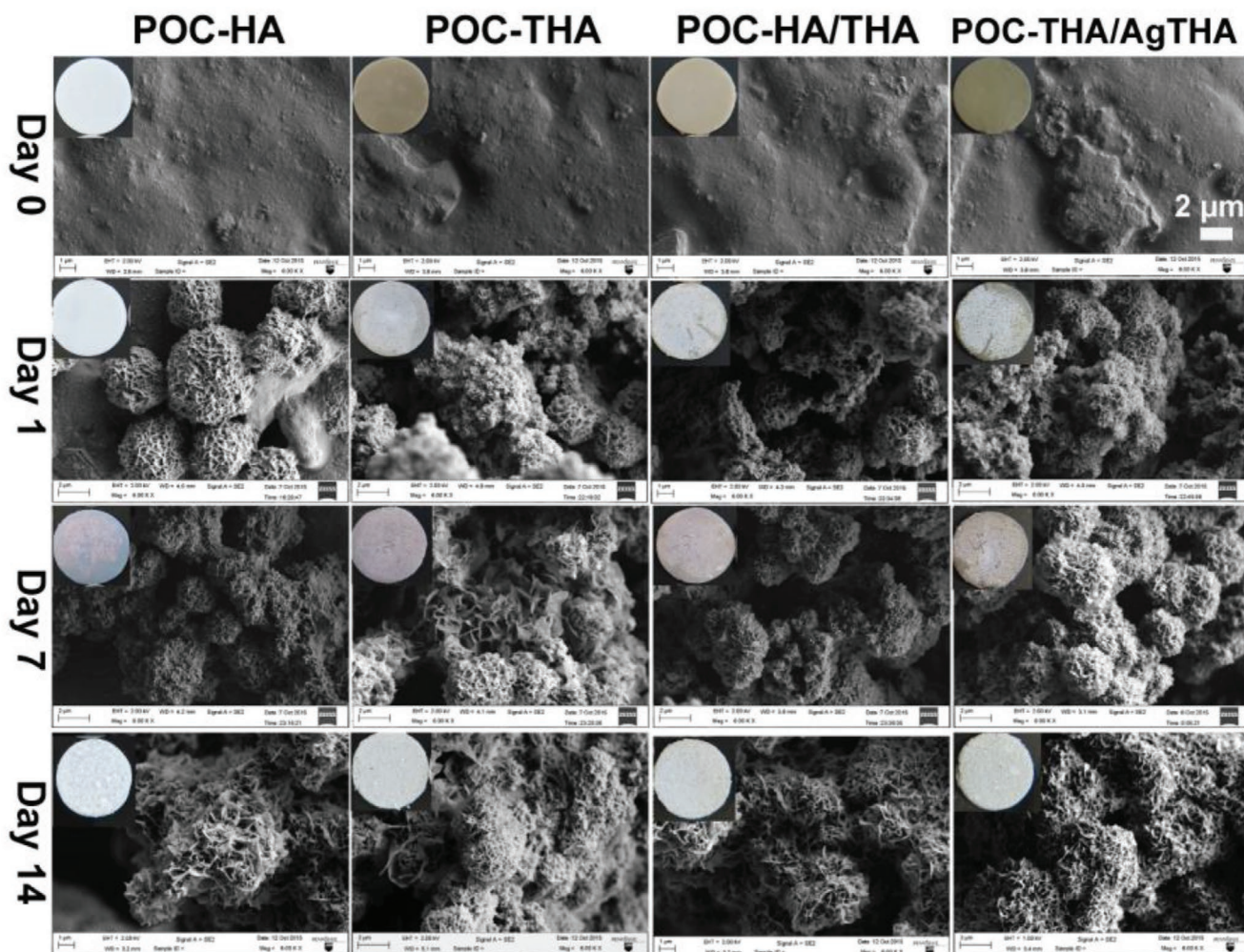


Figure 3. SEM images of mineral deposited on POC-HA, POC-THA, POC-HA/THA 50/50, POC-THA/AgTHA 50/50 composites crosslinked at 80 °C for 3 days plus 120 °C under vacuum for another 3 days in 5 times concentrated simulated body fluid (SBF-5 ×). Insets are photos of the gross morphology of mineralized composites.

and *E. coli* with bacterial survival around 100% for all tested concentrations, and even > 100% for some concentrations (5, 10, 20 mg mL⁻¹ HA against *E. coli*). Both THA and AgTHA exhibited antibacterial activities against *S. aureus*, with MICs of 5 mg mL⁻¹ (Figure 5A; Figure S3, Supporting Information). For tests against *E. coli*, THA exhibited very weak antibacterial activity where 20 mg mL⁻¹ of THA dispersed in agar induced only ≈20% of *E. coli* death (Figure 5B; Figure S3, Supporting Information). The inclusion of Ag NPs led to greatly improved antibacterial activity against *E. coli*; the MIC of AgTHA against *E. coli* was 2.5 mg mL⁻¹ (Figure 5B; Figure S3, Supporting Information). The SEM images of the bacteria taken after 1 day of incubation on agar gels containing THA, AgTHA and HA particles (10, 5, and 10 mg mL⁻¹, respectively) are shown in Figure 5C. These results suggest that the inclusion of both TA and Ag NP are necessary in order to confer considerable innate antibacterial properties against both Gram-positive and Gram-negative bacteria.

The antibacterial performance of composite disks was evaluated by directly exposing composite disks (Φ15 mm × 1 mm) to

S. aureus and *E. coli* suspensions (1 mL) with initial bacteria concentrations of ≈1 × 10⁶ CFU mL⁻¹ (CFU: colony-forming units). The bacterial inhibition ratios were between 20–85% after 24 h (Figure 5D). The contact killing effect of these disks after 24 h was also evaluated by imaging the bacteria attached on the disks with SEM after 24 h (Figure 5E). After 24 h of material exposure, 60–85% of *S. aureus* was inhibited in the POC-THA, POC-HA/THA and POC-THA/AgTHA groups, which was higher than that for POC-HA and PLGA controls (≈22% and ≈3%, respectively), indicating antibacterial activity against *S. aureus* (Figure 5D). The antibacterial property of CTBCs against *S. aureus* is also supported by the contact killing test results (Figure 5E). The weak antimicrobial activity of POC-HA against both *S. aureus* and *E. coli* could be attributed to the innate antimicrobial property of POC.^[49] Against *E. coli*, the POC-THA and POC-HA/THA groups exhibited a slight improvement of antibacterial performance relative to POC-HA (Figure 5D). Consistent with the MIC studies, the inclusion of Ag NPs provided synergy with TA containing groups to increase the bacterial inhibition ratio from ≈10% for POC-HA alone and ≈20% for both POC-THA

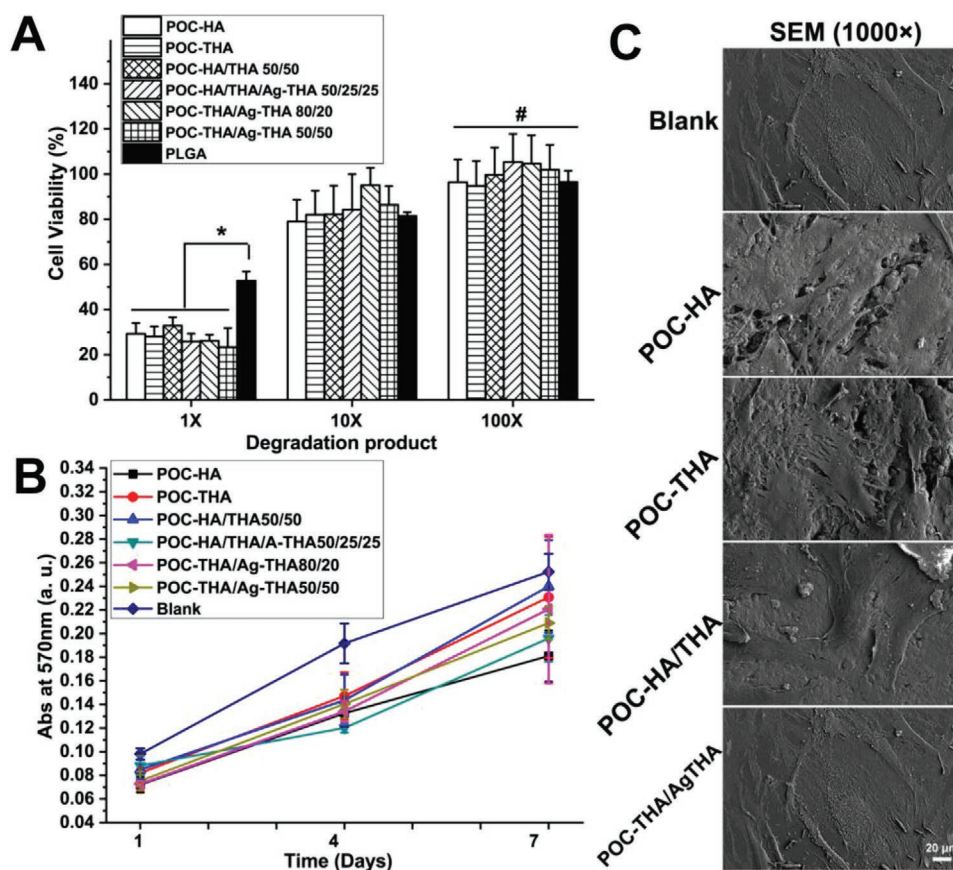


Figure 4. A) Cell cytotoxicity results of the degradation products of different composites at different dilutions using human mesenchymal stem cells (hMSCs); B) Cell proliferation results of hMSCs on different composite disks; C) Images of hMSCs grown on different composite disks for 7 days. # $p > 0.05$, * $p < 0.05$.

and POC-HA/THA to $\approx 40\%$ for POC-THA/AgTHA (Figure 5D). The enhanced antibacterial activity in the Ag NP containing group is also shown in the contact-killing SEM images shown in Figure 5E. The composite antibacterial tests further supported the importance of including both TA and Ag NP in the development of ideal CTBCs with innate antimicrobial properties.

2.6. In Vivo Lumbar Fusion

To assess the in vivo biocompatibility and bone regeneration performance of CTBCs, porous POC-HA/THA and POC-THA/AgTHA scaffolds with a cuboid shape ($10 \times 10 \times 20$ mm, porosity: 65%, pore size: 250–425 μm) were fabricated and evaluated using a lumbar fusion model in rabbits. POC-HA scaffolds and autograft bone (AB) were used as material comparison and positive control, respectively, and a blank negative control group (Control) without any implantation in the bone defect was also used for comparison. The surgical procedure for the lumbar fusion defect is described in the experimental section of the Supporting Information. The application of the implanted scaffold as well as the assembly of the fixation tools is portrayed in Figure 6A with the corresponding X-ray images in Figure 6B.

After 8 and 12 weeks post-surgery, the treated bone tissue sections were harvested for visual observation and micro-computer

tomography (micro-CT) analysis. Histological examination of the decalcified tissue sections was conducted by hematoxylin and eosin (H & E), Masson's trichrome, Safranin O/Fast green staining and osteocalcin (OCN) immunohistochemical staining. Visual observation on the harvested tissue sections at 8 and 12 weeks after surgery (Figure S4, Supporting Information) indicates sufficient fixation of all the implanted grafts. Grafts were surrounded with newly-grown soft tissues, and no signs of infection were observed. In the 2D and 3D images reconstructed by micro-CT analysis (Figure S5, Supporting Information), the in-growth of newly-formed bone tissue from the edge of the bone implantation bed can be observed at 8 weeks after surgery, and increased at week 12 where the boundary between the implantation beds and the implanted bone grafts was less profound. Both visual observation and micro-CT reconstruction suggested enhanced bone tissue regeneration of the three composite treatment groups compared to the blank control group that contained distinct cavities not observed in other groups at week 8 and 12 (Figures S4 and S5, Supporting Information). Quantitative analysis on bone mineral density (BMD, Figure 6C) was consistent with the qualitative observations (Figures S4 and S5, Supporting Information). Although the BMDs of POC-HA/THA and POC-THA/AgTHA groups at week 8 and week 12 were much lower than that of the AB group, there was a significant increase in BMD compared to the blank

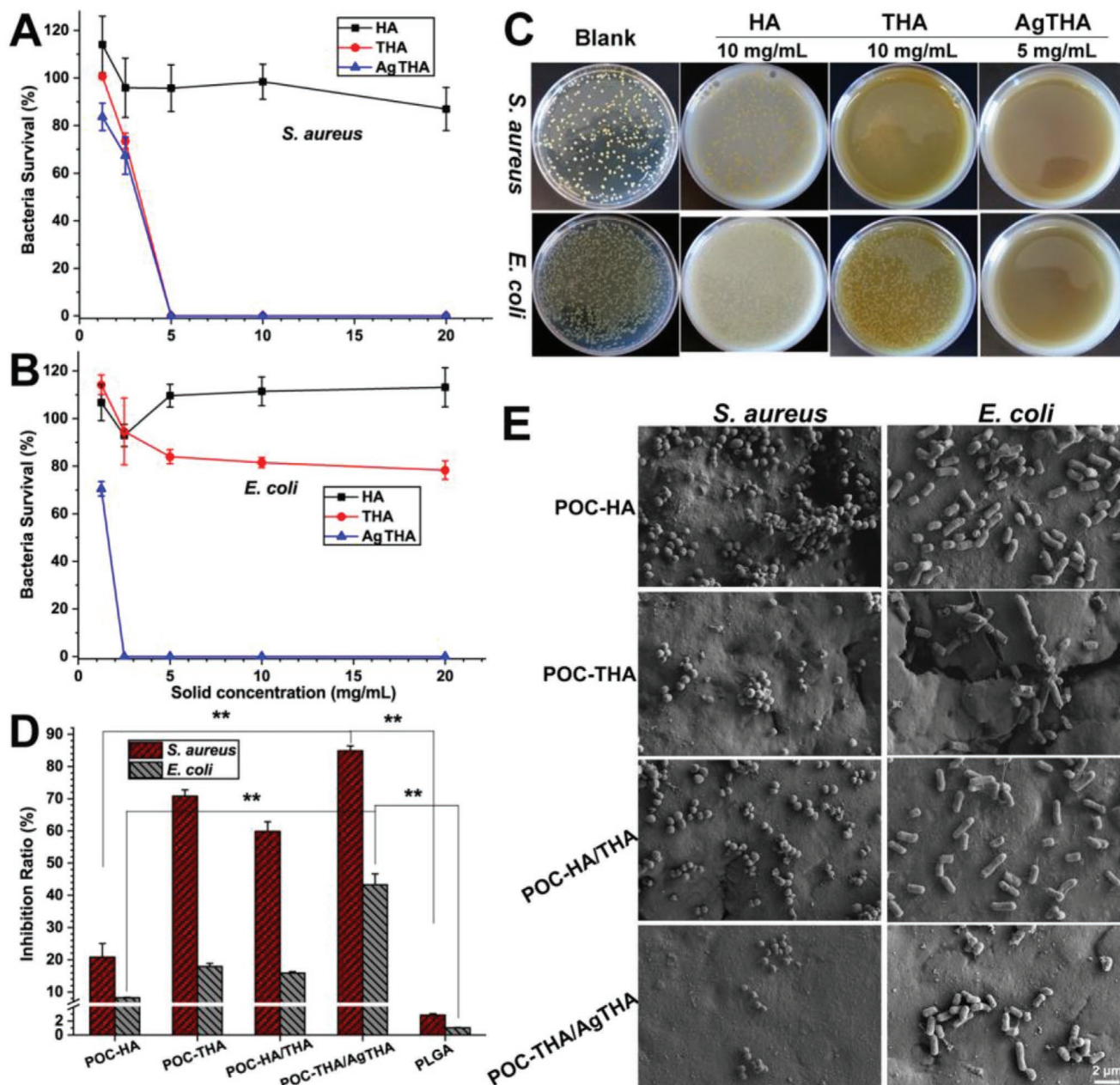


Figure 5. Bacteria survival on agar plates with different concentrations of HA, THA, and AgTHA against A) *S. aureus* and B) *E. coli*. C) Bacterial growth images on blank agar plates and agar plates with HA (10 mg mL⁻¹), THA (10 mg mL⁻¹) and AgTHA (5 mg mL⁻¹); D) Bacterial inhibition ratios (against *S. aureus* and *E. coli* after incubating 1 mL bacteria solution with one circular disk (diameter: 15 mm, thickness: 1 mm) of POC-HA, POC-THA, POC-HA/THA, POC-THA/AgTHA, or PLGA for 24 h and images of bacteria (E) attached on respective disks after 24 h. ***p* < 0.01.

control and POC-HA groups, especially at week 12 (Figure 6C). These results support the favorable osteoconductivity of CTBCs.

Both H & E and Masson's trichrome staining (Figure 7A,B) show new bone and fibrous tissue in-growth into the pores of the composite scaffolds, indicating that all the three kinds of scaffolds can induce *de novo* trabecular bone formation consistent with the micro-CT analysis. In the AB group, newly formed trabeculae can be found at week 12 (Figure 7B) confirming the favorable bone regenerative effects of autograft bone as the gold standard. Compared to POC-HA and blank

control groups, more new bone formation was found in the POC-HA/THA and the POC-THA/AgTHA groups. In the blank control group, the bone defect cavity was mostly filled with fibrous tissue (Figure 7A,B). No significant inflammatory cell infiltration into the surrounding tissue and implanted materials was found at all tested time-points (Figure 7A). Cartilage was detected in the newly formed bone tissue of all five groups (Figure 7B), which is most evident by the Safranin O and Fast Green staining images where cartilage appears orange while bone tissue stains green (Figure 7C). For the AB group, cartilage

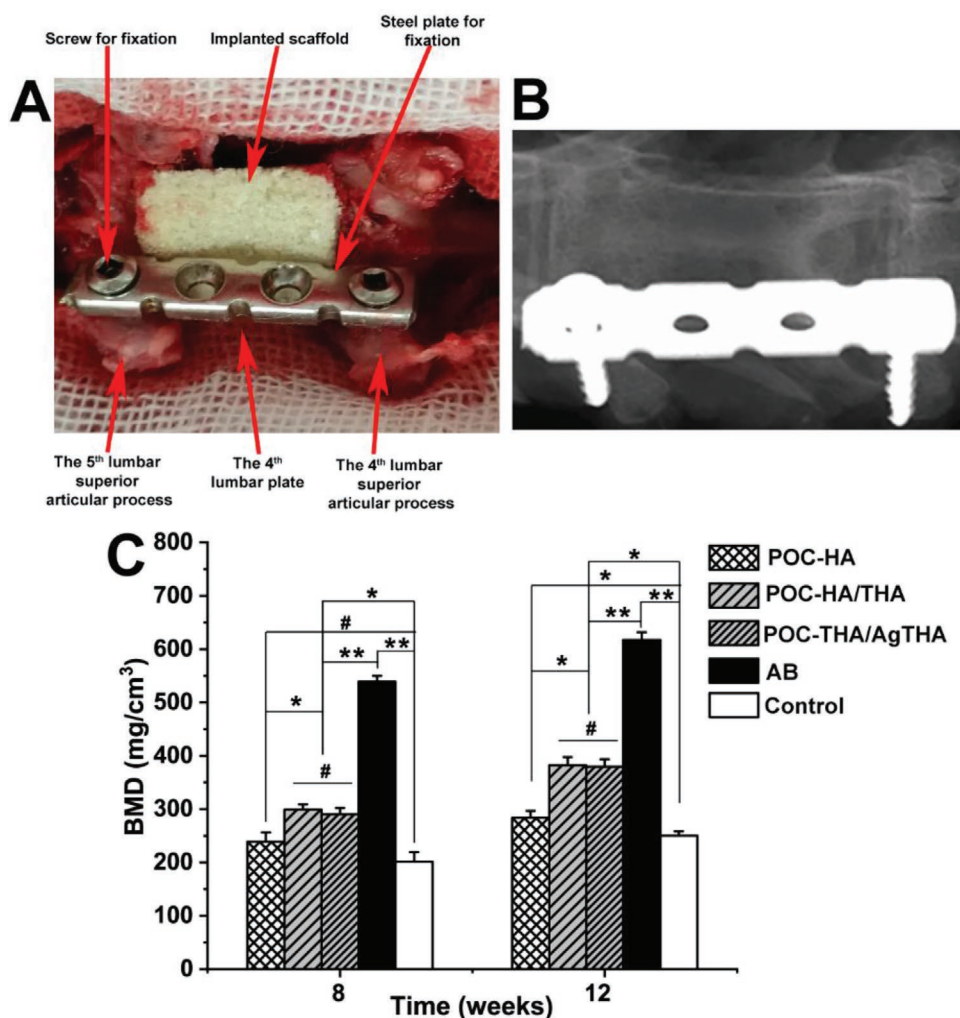


Figure 6. A) Photo illustrating the lumbar fusion surgery: the 4th (L4) lumbar plate was removed to create a 20 × 10 mm defect, where an implanted material (composite scaffold or autograft bone) was imbedded. A steel plate was fixed on the 4th (L4) and 5th (L5) lumbar superior articular processes using two steel screws to prevent movement of the implanted material and provide mechanical support during the lumbar fusion process; the X-ray image of the surgical section after material implantation and steel plate fixation. B) The penetration of the two steel screws into the lumbar superior articular processes can be clearly observed. C) Bone mineral densities (BMDs) obtained from micro-CT analysis of different samples at 8 and 12 weeks post-lumbar fusion surgery (AB: autograft bone; Control: no implantation in the defect). # $p > 0.05$, * $p < 0.05$, ** $p < 0.01$.

tissue surrounded the implanted autograft bone at week 8 but was less evident by week 12 (Figure 7C) indicating that cartilage formation is an inherent part of early bone formation in the lumbar fusion process. More cartilage tissue was observed in the POC-HA/THA and POC-THA/AgTHA groups than in the POC-HA group (Figure 7C), suggesting that CTBCs may promote lumbar fusion through endochondral ossification. Osteocalcin (OCN) is a characteristic indicator for mature osteoblasts.^[44] Thus, OCN immunohistochemical staining can be used to reflect the osteoinductivity of bone implants by highlighting the number of mature osteoblasts in a given sample. At week 8, a large number of OCN-positive osteoblasts in the AB group was observed on the surface of the newly formed trabeculae between the edge of the bone defect and the graft, indicating the high presence and potential activity of osteoblasts (Figure 7D). In contrast, in the blank control group, very few OCN-positive osteoblasts were found relative to the

treatment groups and were confined to the edges of the defect (Figure 7D). OCN-positive osteoblasts were similarly observed on the surface of the new trabeculae in the three composite bone grafts, suggesting that both CTBCs and normal citrate-based bone composites can promote the differentiation of osteogenic precursor cells, exhibiting favorable osteoinductivity.

The *in vivo* study results further confirm the biocompatibility of CTBCs as well as indicate favorable osteoconductivity and osteoinductivity of CTBCs to promote osteogenesis in lumbar fusion compared to blank control and POC-HA groups.

3. Conclusion

In conclusion, a family of citrate-based and tannin-bridged bone composites (CTBCs) was developed by reacting tannic acid (TA) with hydroxyapatite (HA) particles to strongly

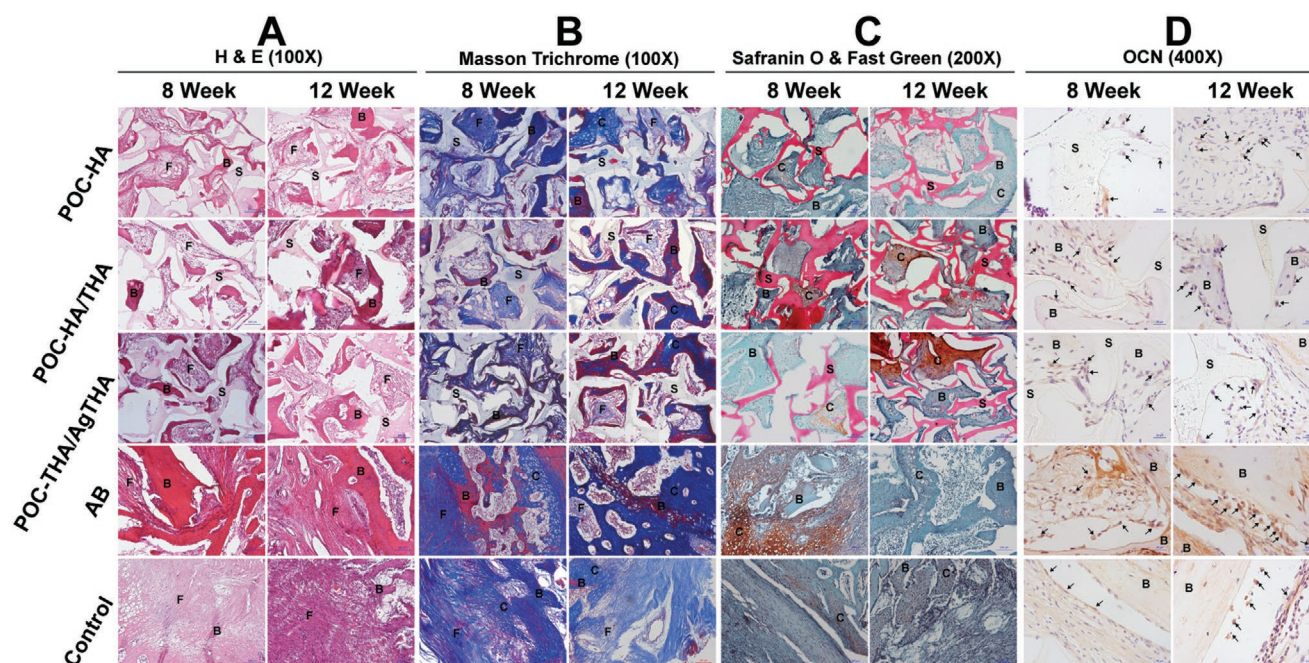


Figure 7. Representative images of A) H & E (hematoxylin and eosin), B) Masson Trichrome, C) Safranin O and Fast Green and D) OCN immunohistochemical (OCN: osteocalcin), staining at week 8 and 12 of the decalcified tissue sections containing the implanted materials, including POC-HA, POC-HA/THA, POC-THA/AgTHA composite scaffolds and autograft bone (AB). A blank control sample (Control) without any implantation in the defect was also tested. B: bone, C: cartilage, F: fibrous tissue, S: scaffold. In the OCN staining images, the black arrows indicate OCN positive cells.

adhere TA to the HA surface followed by chemical binding with poly(octamethylene citrate) (POC), the representative citrate-based biodegradable polymer, during the subsequent thermal crosslinking process. TA effectively bridged the inorganic and organic composites phases, improving the compression strengths of the TA containing composite scaffolds up to 325 MPa, exceeding the maximum strength of native bone. The surface coating of TA and in situ formed silver nanoparticles (Ag NP) on HA endowed the modified HA and CTBCs with considerable antimicrobial performance, enhanced biomineralization, favorable biocompatibility, and increased cell adhesion and proliferation. In vivo lumbar fusion using porous CTBCs further confirmed their enhanced osteoconductivity and osteoinductivity relative to blank and POC-HA controls. Immobilized TA also preserves multifunctional reactive groups for surface bioconjugation to further improve the bioactivity of CTBCs. The tannin-mediated adhesion and chemical reaction strategy provides a new paradigm to mimic the integrated organic/inorganic structure of natural bone, and to utilize the cell adhesion, biomineralization and antimicrobial functions of polyphenols for the promotion of bone regeneration lacking in currently available bone-mimetic materials. This versatile application paradigm may be widely expanded into other bio-related applications to develop high performance composites.

Supporting Information

Supporting Information is available from the Wiley Online Library or from the author.

Acknowledgements

J.G., X.T., and D.X. contributed equally to this work.

Conflict of Interest

The authors declare no conflict of interest.

Keywords

biomimetics, bone regeneration, citrate-based biodegradable polymers, composite materials, tannin-mediated adhesion

Received: March 16, 2020

Revised: March 29, 2020

Published online:

- [1] M. Dang, L. Saunders, X. Niu, Y. Fan, P. X. Ma, *Bone Res.* **2018**, *6*, 25.
- [2] K. Zhang, S. Wang, C. Zhou, L. Cheng, X. Gao, X. Xie, J. Sun, H. Wang, M. D. Weir, M. A. Reynolds, N. Zhang, Y. Bai, H. H. K. Xu, *Bone Res.* **2018**, *6*, 31.
- [3] T.-M. De Witte, L. E. Fratila-Apachitei, A. A. Zadpoor, N. A. Peppas, *Regener. Biomater.* **2018**, *5*, 197.
- [4] R. J. O'Keefe, J. Mao, *Tissue Eng., Part B* **2011**, *17*, 389.
- [5] D. Sun, Y. Chen, R. T. Tran, S. Xu, D. Xie, C. Jia, Y. Wang, Y. Guo, Z. Zhang, J. Guo, J. Yang, D. Jin, X. Bai, *Sci. Rep.* **2015**, *4*, 6912.
- [6] J. Tang, J. Guo, Z. Li, C. Yang, D. Xie, J. Chen, S. Li, S. Li, G. B. Kim, X. Bai, Z. Zhang, J. Yang, *J. Mater. Chem. B* **2015**, *3*, 5569.
- [7] A. M. Schwartz, M. L. Schenker, J. Ahn, N. J. Willett, *J. Orthop. Res.* **2017**, *35*, 1855.

- [8] N. Shao, J. Guo, Y. Guan, H. Zhang, X. Li, X. Chen, D. Zhou, Y. Huang, *Biomacromolecules* **2018**, *19*, 3637.
- [9] D. Xie, J. Guo, M. R. Mehdizadeh, R. T. Tran, R. Chen, D. Sun, G. Qian, D. Jin, X. Bai, J. Yang, *J. Mater. Chem. B* **2015**, *3*, 387.
- [10] X. Qiu, L. Chen, J. Hu, J. Sun, Z. Hong, A. Liu, X. Chen, X. Jing, *J. Polym. Sci., Part A: Polym. Chem.* **2005**, *43*, 5177.
- [11] Z. Wang, L. Chen, Y. Wang, X. Chen, P. Zhang, *ACS Appl. Mater. Interfaces* **2016**, *8*, 26559.
- [12] M. Diba, W. A. Camargo, M. Brindisi, K. Farbod, A. Klymov, S. Schmidt, M. J. Harrington, L. Draghi, A. R. Boccaccini, J. A. Jansen, J. J. P. van den Beucken, S. C. G. Leeuwenburgh, *Adv. Funct. Mater.* **2017**, *27*, 1703438.
- [13] D. Zhang, X. Wu, J. Chen, K. Lin, *Bioact. Mater.* **2018**, *3*, 129.
- [14] Y. Cui, T. Zhu, A. Li, B. Liu, Z. Cui, Y. Qiao, Y. Tian, D. Qiu, *ACS Appl. Mater. Interfaces* **2018**, *10*, 6956.
- [15] S. Nagarajan, H. Belaid, C. Pochat-Bohatier, C. Teyssier, I. Iatsunskiy, E. Coy, S. Balme, D. Cornu, P. Miele, N. S. Kalkura, V. Cavaillès, M. Bechelany, *ACS Appl. Mater. Interfaces* **2017**, *9*, 33695.
- [16] W. Limin, *Biomaterials* **2010**, *31*, 3976.
- [17] J. Wei, A. Liu, L. Chen, P. Zhang, X. Chen, X. Jing, *Macromol. Biosci.* **2009**, *9*, 631.
- [18] J. Wei, P. He, A. Liu, X. Chen, X. Wang, X. Jing, *Macromol. Biosci.* **2009**, *9*, 1237.
- [19] H. Lee, B. P. Lee, P. B. Messersmith, *Nature* **2007**, *448*, 338.
- [20] M. Mehdizadeh, H. Weng, D. Gyawali, L. Tang, J. Yang, *Biomaterials* **2012**, *33*, 7972.
- [21] J. Guo, W. Wang, J. Hu, D. Xie, E. Gerhard, M. Nisic, D. Shan, G. Qian, S. Zheng, J. Yang, *Biomaterials* **2016**, *85*, 204.
- [22] J. Guo, G. B. Kim, D. Shan, J. P. Kim, J. Hu, W. Wang, F. G. Hamad, G. Qian, E. B. Rizk, J. Yang, *Biomaterials* **2017**, *112*, 275.
- [23] J. Guo, W. Sun, J. P. Kim, X. Lu, Q. Li, M. Lin, O. Mrowczynski, E. B. Rizk, J. Cheng, G. Qian, J. Yang, *Acta Biomater.* **2018**, *72*, 35.
- [24] X. Lu, S. Shi, H. Li, E. Gerhard, Z. Lu, X. Tan, W. Li, K. M. Rahn, D. Xie, G. Xu, F. Zou, X. Bai, J. Guo, J. Yang, *Biomaterials* **2020**, *232*, 119719.
- [25] L. Xu, L. K.-G. Neoh, E.-T. Kang, *Prog. Polym. Sci.* **2018**, *87*, 165.
- [26] Y. Liu, H. Meng, Z. Qian, N. Fan, W. Choi, F. Zhao, B. P. Lee, *Angew. Chem., Int. Ed.* **2017**, *56*, 4224.
- [27] B. P. Lee, P. B. Messersmith, J. N. Israelachvili, J. H. Waite, *Annu. Rev. Mater. Res.* **2011**, *41*, 99.
- [28] C. Rodriguez-Emmenegger, C. M. Preuss, B. Yameen, O. Pop-Georgievski, M. Bachmann, J. O. Mueller, M. Bruns, A. S. Goldmann, M. Bastmeyer, C. Barner-Kowollik, *Adv. Mater.* **2013**, *25*, 6123.
- [29] T. S. Sileika, D. G. Barrett, R. Zhang, K. H. A. Lau, P. B. Messersmith, *Angew. Chem., Int. Ed.* **2013**, *52*, 10766.
- [30] J. Saiz-Poseu, J. Mancebo-Aracil, F. Nador, F. Busqué, D. Ruiz-Molina, *Angew. Chem., Int. Ed.* **2018**, *57*, 2.
- [31] C. Lee, S.-H. Kim, J.-H. Jang, S.-Y. Lee, *Sci. Rep.* **2017**, *7*, 13797.
- [32] L. He, D. Deng, X. Zhou, L. Cheng, J. M. ten Cate, J. Li, X. Li, W. Crielaard, *J. Biomed. Mater. Res., Part B* **2015**, *103*, 1525.
- [33] J. Ryu, S. H. Ku, H. Lee, C. B. Park, *Adv. Funct. Mater.* **2010**, *20*, 2132.
- [34] D. J. Lee, Y.-T. Lee, R. Zou, R. Daniel, C.-C. Ko, *Sci. Rep.* **2017**, *7*, 12984.
- [35] D. J. Lee, H. C. Tseng, S. W. Wong, Z. Wang, M. Deng, C.-C. Ko, *Bone Res.* **2015**, *3*, 15020.
- [36] M. J. Roman, E. A. Decker, J. M. Goddard, *Colloid Interface Sci. Commun.* **2016**, *13*, 10.
- [37] X. Yang, P. Huang, H. Wang, S. Cai, Y. Liao, Z. Mo, X. Xu, C. Ding, C. Zhao, J. Li, *Colloids Surf., B* **2017**, *160*, 136.
- [38] K. Fujita, K. Kuge, N. Ozawa, S. Sahara, K. Zaiki, K. Nakaoji, K. Hamada, Y. Takenaka, T. Tanahashi, K. Tamai, Y. Kaneda, A. Maeda, *PLoS One* **2015**, *10*, e0144166.
- [39] L. C. Costello, R. B. Franklin, M. A. Reynolds, M. Chellaiah, *Open Bone J.* **2012**, *4*, 27.
- [40] J. Guo, Z. Xie, R. T. Tran, D. Xie, D. Jin, X. Bai, J. Yang, *Adv. Mater.* **2014**, *26*, 1906.
- [41] Y. Guo, R. T. Tran, D. Xie, Y. Wang, D. Y. Nguyen, E. Gerhard, J. Guo, J. Tang, Z. Zhang, X. Bai, J. Yang, *J. Biomed. Mater. Res., Part A* **2015**, *103*, 772.
- [42] Y. Y. Hu, A. Rawal, K. Schmidt-Rohr, *Proc. Natl Acad. Sci. USA* **2010**, *107*, 22425.
- [43] E. Davies, K. H. Müller, W. Wong, C. J. Pickard, D. G. Reid, J. N. Skepper, M. J. Duer, *Proc. Natl. Acad. Sci. USA* **2014**, *111*, E1354.
- [44] C. Ma, X. Tian, J. P. Kim, D. Xie, X. Ao, D. Shan, Q. Lin, M. R. Hudock, X. Bai, J. Yang, *Proc. Natl. Acad. Sci. USA* **2018**, *115*, E11741.
- [45] J. Yang, A. R. Webb, G. A. Ameer, *Adv. Mater.* **2004**, *16*, 511.
- [46] Q. Liu, J. R. de Wijn, C. A. van Blitterswijk, *J. Biomed. Mater. Res.* **1998**, *40*, 490.
- [47] Q. Liu, J. R. de Wijn, D. Bakker, M. van Toledo, C. A. van Blitterswijk, *J. Mater. Sci. Mater. Med.* **1998**, *9*, 23.
- [48] P. Uznanski, J. Zakrzewska, F. Favier, S. Kazmierski, E. Bryszewska, *J. Nanopart. Res.* **2017**, *19*, 121.
- [49] L.-C. Su, Z. Xie, Y. Zhang, K. T. Nguyen, J. Yang, *Front. Bioeng. Biotechnol.* **2014**, *2*, 23.

ADVANCED FUNCTIONAL MATERIALS

Supporting Information

for *Adv. Funct. Mater.*, DOI: 10.1002/adfm.202002438

Citrate-Based Tannin-Bridged Bone Composites for Lumbar Fusion

Jinshan Guo, Xinggui Tian, Denghui Xie, Kevin Rahn, Ethan Gerhard, Michelle Laurel Kuzma, Dongfang Zhou, Cheng Dong, Xiaochun Bai, Zhihui Lu,* and Jian Yang**

Copyright WILEY-VCH Verlag GmbH & Co. KGaA, 69469 Weinheim, Germany, 2020.

Supporting Information

Citrate-based tannin-bridged bone composites for lumbar fusion

Jinsahn Guo,[#] Xinggui Tian,[#] Denghui Xie,[#] Kevin Rahn, Ethan Gerhard, Michelle Laurel Kuzma, Dongfang Zhou, Cheng Dong, Xiaochun Bai, Zhihui Lu,* and Jian Yang**

Prof. J. Guo, X. Tian, Prof. D. Xie, Prof. Zhou, Prof. X. Bai, Prof. Z. Lu
Department of Histology and Embryology, School of Basic Medical Sciences, Department of Orthopedic Surgery, The Third Affiliated Hospital of Southern Medical University, Southern Medical University, Guangzhou, China; Academy of Orthopedics of Guangdong province, Guangdong Provincial Key Laboratory of Bone and Joint Degeneration Diseases, Guangzhou, China

X. Tian,
Department of Spine Surgery, The Affiliated Hospital of Southwest Medical University, Luzhou, Sichuan 646000, China

Prof. D. Zhou,
School of Pharmaceutical Sciences, Southern Medical University, Guangzhou, 510515, China

Prof. X. Bai,
Department of Biology, School of Basic Medical Sciences, Southern Medical University, Guangzhou, 510515, China

*Corresponding Emails: jxy30@psu.edu (Prof. J. Yang, Tel.: +1-814-865-1278),
luzhihui107@sohu.com (Prof. Z. Lu), baixc15@smu.edu.cn (Prof. X. Bai)

Keywords: tannin, citrate, biomimetics, composite materials, bone regeneration

Experimental Section

Materials

Hydroxyapatite (HA) powder, tannic acid (TA), citric acid (CA), 1,8-octanediol, silver nitrate (AgNO_3) and other chemicals were all purchased from Sigma-Aldrich and used without further purification.

General measurements

Attenuated total reflectance-Fourier transform infrared (ATR-FTIR) spectra were measured on a Nicolet 6700 FTIR spectrometer using modified and unmodified HA powder directly on a ZnSe crystal with air as background. X-ray diffraction (XRD) measurements of modified and unmodified HA samples were performed on a PANalytical Empyrean X-ray powder diffractometer (Cu $K\alpha$ radiation, 45 kV, 40 mA) with the detection range from 5 to 80 degrees. X-ray photoelectron spectroscopy (XPS) was taken on a Physical Electronics VersaProbe II electron spectrometer using Mg KR (1253.6 eV) as the X-ray excitation source at room temperature. Scanning electron microscopy (SEM) images and energy dispersive spectroscopy (EDS) data were obtained using Zeiss Sigma VP-FESEM in the Huck institute of the Life Science at The Pennsylvania State University.

Hydroxyapatite modification

Tannic acid (TA) was coated on the surface of hydroxyapatite (HA) to create TA modified hydroxyapatite (THA) via a one-step reaction in Tris-HCl buffer (pH 8.5). First, HA (20 g) was charged to a 500 mL round bottom flask. TA (5 g) was dissolved in 50 mL pH 8.5 Tris-HCl buffer solution and combined with HA in the 500 mL flask. Another 150 mL of Tris-HCl buffer (pH 8.5) was added to the solution. The flask was sealed with a stopper and the solution was stirred at 1200 rpm and room temperature for 24 hours. The crude THA particles were purified via centrifugation. Briefly, the dispersed particles in buffer solution were centrifuged at 3000 rpm for 5 minutes. After centrifuging, the supernatant was discarded and the particles were resuspended in deionized (DI) water and dispersed using an ultrasonic water bath (50-60 Hz) for 5 minutes. The dispersed particles were again centrifuged at 3000 rpm for 5 minutes and the supernatant was discarded. This purification process was repeated 5

times until the supernatant was colorless indicating full removal of unreacted TA. After purification, the THA particles were lyophilized for 3 days. Dry particles were then grounded to achieve uniform size.

Silver and TA modified HA (AgTHA) was synthesized via a similar process. HA (20 g) was added to a 500 mL round bottom flask and 5 g TA was dissolved in 50 mL pH 8.5 Tris-HNO₃ buffer solution. Then 0.5 g AgNO₃ was dissolved in 15 mL pH 8.5 Tris-HNO₃ buffer solution. The dissolved TA and AgNO₃ were added to the flask with another 150 mL of the Tris-HNO₃ (pH 8.5) buffer solution. The flask was stoppered and the reaction mixture was stirred at 1200 rpm and room temperature for 24 hours. Tris-HNO₃, rather than Tris-HCl buffer, was used to prevent the formation of silver chloride (AgCl) precipitate. The purification process was the same as that of THA.

Synthesis of poly(octamethylene citrate) (POC) prepolymer

POC prepolymer was synthesized using a one-pot polycondensation process as described in previous literature;^[1-3] the ratio of citric acid (CA) to 1, 8-octanediol (OD) used was 1.0:1.1. After synthesis, the obtained POC prepolymer was dissolved in 1,4-dioxane to make a 30 wt% POC solution for further use.

Composite disk fabrication

POC composites with varying ratios of HA, THA and/or AgTHA were fabricated for degradation, biomineralization, antimicrobial and cell proliferation studies. First, 30 wt% POC prepolymer solution, HA, THA and/or AgTHA were weighed and mixed in a Teflon dish at the following ratios: POC-HA 60 wt% (weight ratio of HA to the total weight of POC dry polymer and HA), POC-THA 60 wt%, POC-HA/THA 60 wt% 50/50 (ratio of HA/ THA = 50/50), POC-THA/AgTHA 60 wt% 50/50, POC-THA/AgTHA 60 wt% 80/20, and POC-HA/THA/AgTHA 60 wt% 50/25/25. The resulting composite slurry was uniformly mixed during solvent evaporation via vigorous stirring until a homogenous putty was achieved. The composite putty was kneaded into a ball and stored in a sealable plastic bag to prevent

evaporation of remaining solvent. A hand rolling press was used to make composite films approximately 10 mm thick. The films were lyophilized for 24 hours to remove any remaining solvent. Finally, the composites were further pressed into 1 mm thick films using the same rolling press. Disks were cut from the films using a 15 mm diameter circular metal punch. Smaller composite disks (7 mm in diameter, 0.5 mm in thickness) were also prepared for degradation studies. Disks were then crosslinked at specific crosslinking conditions (80 °C, 3 days, 120 °C vacuum, 1 day; 80 °C, 3 days, 120 °C vacuum, 3 days; 100 °C, 3 days, 120 °C vacuum, 1 day).

Composite cylinder fabrication and mechanical testing

Using the previously prepared 1 mm thick composite films, thin strips of the composite (0.81 g composite per 12 mm height \times Φ 6 mm cylinder) were loaded into 6 mm inner diameter Teflon tubing and steel end caps (6 mm outer diameter) were fit into each end of the Teflon tubing to fabricate composite cylinders with a height of approximately 12 mm. The loaded Teflon tube was fit into a steel cylindrical mold and was then pressed to 3 tons with a manual hydraulic press. The metal molds were then clamped with C-clamps to prevent expansion of the composite and thermally crosslinked at the desired conditions (80 °C, 3 days, 120 °C vacuum, 1 day; 80 °C, 3 days, 120 °C vacuum, 3 days; 100 °C, 3 days, 120 °C vacuum, 1 day). Cylinders were removed from the molds after the initial 3 days of crosslinking and allowed to crosslink for the remaining time out of mold. After that, the crosslinked composite cylinders were slightly sanded to obtain smooth surfaces.

Mechanical characterization of the POC/HA, POC/THA and POC/AgTHA composites was completed by submitting fabricated cylinders to a uniaxial compressive load in an Instron 5966 mechanical tester fitted with a 10 kN load cell (Instron, Norwood, MA). Eight cylinders for each composite formulation and crosslinking condition were tested and averaged to determine compressive strength, modulus of elasticity (Young's Modulus) and strain at

break. Young's modulus was determined by the slope of the stress-strain curve from 0% to 10% elongation.

For comparison, POC/TA films (thickness: 0.15 mm) were made by mixing POC prepolymer and TA (weight ratios of POC/TA (w/w) = 90/10, 85/15, 80/20) followed by crosslinking at 100 °C for 3 days, while POC/TA-HA composite cylinders ($\Phi 6$ mm \times 12 mm) were made by compositing POC/TA (w/w = 90/10, 85/15, 83/17) with HA followed by crosslinking at 80 °C for 3 days and then 120 °C vacuum for 1 day. The tensile tests and compression tests on the POC/TA films and POC/TA composite cylinders were conducted respectively, and the results are shown in Figure S1.

Degradation study

For degradation studies, composite disks ($\Phi 7$ mm, 1 mm thickness) were placed in plastic tubes containing 10 mL of phosphate buffered saline (PBS, pH 7.4) and incubated at 37 °C. The PBS buffer was changed every two weeks. After pre-set incubation times, specimens were washed thoroughly with DI water (at least 4 times) to remove residual salt before freeze-drying. Mass loss was calculated by Equation (1). Here W_0 and W_1 are the initial weight and the weight after degradation, respectively. For each sample, at least five specimens were tested and the results were averaged and presented as the mean \pm standard deviation.

$$\text{Mass Loss (\%)} = \frac{W_0 - W_1}{W_0} \times 100 \quad (1)$$

The pH values of the PBS buffer solutions after degradation were recorded also recorded.

Biom mineralization

To evaluate the *in vitro* biom mineralization capability of THA, AgTHA and respective composites with POC, THA or AgTHA coated silicon wafers as well as the disk-shaped composites consisting of POC-THA, POC-HA/THA (50/50) and POC-THA/AgTHA (50/50) ($\Phi 15$ mm \times 1 mm) were prepared. All composites for the biom mineralization studies were crosslinked at 80 °C for 3 days plus 120 °C vacuum for an additional 3 days. HA coated

silicon wafers and POC-HA were used as controls for particle and composite groups, respectively. The samples were immersed in simulated body fluid (SBF), which was prepared as described previously.^[4] To accelerate the mineralization process, concentrated SBF was used, in which the concentration of inorganic ions was five times that of human blood plasma (SBF-5×). The samples were immersed in 10 mL of SBF-5× and incubated at 37 °C for 1, 4, 7 days or 1, 7, 14 days for particle samples or composite disks, respectively. Half of the volume of the SBF-5× solution was replaced with fresh solution every other day. At each preset time point, the specimens (n = 5) were removed from solution, washed gently with DI water to remove inorganic ions from the sample surfaces, and air-dried. Next, the specimens were sputter-coated with gold (5 nm thick) and observed by scanning electron microscopy (SEM) using Zeiss Sigma VP-FESEM. Elemental analysis of the mineralized composites was conducted by energy dispersive X-ray spectroscopy (EDS) to determine the composition and elemental ratio of the deposited minerals.

Biocompatibility of composite films

The biocompatibility of the tested composites, including POC-HA, POC-THA and POC-THA/AgTHA, was assessed using the MTT (methylthiazolyl-diphenyl-tetrazolium bromide) assay and SEM imaging to study cytotoxicity of the degradation products and cell proliferation on the surface of composite disks, respectively. Passage 5-10 human mesenchymal stem cells (hMSCs, ATCC® PCS-500-012™) were used.

To measure cytotoxicity of the degradation products of the tested composites, composite film samples (1 g each) were degraded in 10 mL 0.2 M NaOH until full degradation was achieved, followed by pH adjustment to 7.4 with sterilization through a 0.2 μm Teflon filter. The sterilized solution was diluted to 1×, 10× and 100× solutions with sterile PBS. POC-HA 60wt% and commercially available poly(lactic acid-co-glycolic acid) (PLGA, LA/GA = 50/50, 60 kDa, Polysciotech) were used as a controls. hMSCs (200 μL, 5×10⁴ cells/mL) dispersed in growth medium (Dulbecco's modified eagle's medium (DMEM), 10% (v/v) fetal bovine

serum (FBS), 1% (v/v) antibiotic antimycotic solution (100×)) were seeded in each well of 96-well plates. The cells were incubated (37°C, 5% CO₂, 95% RH) to attach overnight. Afterwards, 20 µL of the sterilized solution of the degradation products (1×, 10× and 100× diluted in PBS) were added into the wells of 96-well plates. The cells were cultured for another day then underwent the MTT assay as specified by the manufacturer. For each cohort, at least 6 samples were measured and the results were averaged.

hMSC proliferation on composites was evaluated by MTT assay and SEM imaging with POC-HA 60wt% as control. Cells were seeded onto composite disks (Φ15mm, 1 mm thickness) in 24-well plates (5000 cells/well) with growth medium and cultured for 7 days. The MTT assay was conducted at days 1, 3, and 7, and SEM imaging was performed on the day 7 samples. For each sample, at least 4 disks were tested and the results were averaged.

Antibacterial performance of POC-THA, POC-HA/THA and POC-THA/AgTHA

Bacterial Incubation

Antimicrobial tests were performed against *Staphylococcus aureus* (*S. aureus*, ATCC® 6538TM) and *Escherichia coli* (*E. coli*, ATCC® 25922TM) purchased from the American Type Culture Collection and cultivated following standard safety protocols. Tryptic soy agar (Cat. #: C7121TM) and tryptic soy broth (Cat. #: C7141TM) purchased from Criterion were used for the *S. aureus* culture, while Luria Broth Base (LB broth, Cat. #: 12795-027) and select agar (Cat. #: 30391-023) purchased from Invitrogen were used for the *E. coli* culture. Tryptic soy broth and LB broth were sterilized then *S. aureus* and *E. coli* were cultivated in the corresponding broth at 37 °C overnight at a speed of 150 rpm on a rotary shaker. The bacterial suspensions were diluted to desired concentrations before use.

Minimal inhibitory concentrations (MICs) of HA, THA, and AgTHA particles against bacteria

An agar macrodilution method was used to determine the MICs of THA and AgTHA particles against *S. aureus* and *E. coli*; HA was used as control. Briefly, preset concentrations of HA,

THA, and AgTHA particles were made using DI water and the corresponding agar mix for *S. aureus* (Tryptic soy agar) or for *E. coli* (LB broth and agar). The solutions were mixed in glass vials, capped with foil, and autoclaved to sterilize and liquefy the agar/particle mix. The liquid samples were placed into 6-well plates (3 mL/well) and allowed to solidify. Particle concentrations of 20, 10, 5, 2.5, and 1.25 mg/mL were prepared and blank agar was used as control. After solidification, bacterial suspensions were evenly spread on the wells of 6-well plates and the extra broth was allowed to evaporate. The plates were incubated at 37 °C for 24 hours and bacterial colonies were counted using the ImageJ cell counter, ensuring that the bacterial population fell into the countable range of 25~250 CFUs/well (CFU: colony forming unit) as recommended by the FDA Bacterial Analytical Manual (BAM). For different bacteria, a standard curve of CFUs/mL vs. optical density (OD) value at 600 nm was first obtained to roughly predict bacterial concentration. The bacteria survival was calculated by equation (2):

$$\text{Bacteria survival (\%)} = (N/N_c) \times 100 \quad (2)$$

where N is the bacterial colony number in the sample-containing well, and N_c is the bacterial colony number in blank agar well.

For each of the particle concentrations, at least 3 samples were tested and the results were averaged. For THA and AgTHA, the lowest particle concentration with 0% bacteria survival was determined to be the MIC against the tested bacteria.

Antibacterial performance of POC-THA, POC-HA/THA and POC-THA/AgTHA composite disks

The antibacterial performance of POC-THA, POC-HA/THA, and POC-THA/AgTHA composite disks was evaluated by direct exposure to bacterial suspensions of both *S. aureus* and *E. coli*. Briefly, composite disks (Φ 15mm, 1 mm thickness) were placed into the wells of 24-well plates followed by the addition of 1 mL bacteria suspension ($\sim 1 \times 10^6$ CFUs/mL) in each well. POC-HA and PLGA composite disks were used as positive and negative controls,

respectively, while the blank sample contained the pure bacteria suspension only. The bacteria suspensions were cultured at 37 °C with a shaking speed of 150 rpm for 24 hours before being removed for OD testing at 600 nm. The bacterial inhibition ratio was calculated through equation (3):

$$\text{Bacterial inhibition ratio (\%)} = 100 - 100 \times \frac{A - A_0}{A_b - A_0} \quad (3)$$

where A_0 is the initial OD value of the bacterial suspension, A is the OD value of the bacterial suspension for composite sample after 24 hours of culture, and A_b is the OD value of the blank sample after 24 hours of incubation.

The bacteria that grew on the composite disks were also characterized by SEM imaging (Figure 5E).

Composite scaffold fabrication and *in vivo* study

Composite scaffold fabrication

Porous composite scaffolds (10 × 10 × 20 mm) of POC-HA (HA content: 60 wt%), POC-HA/THA (HA + THA content: 60%, ratio of HA/THA = 50/50), and POC-THA/AgTHA (THA + AgTHA content: 60%, ratio of THA/AgTHA = 80/20) with a porosity of 65% and pore size of 250-425 μm were fabricated using the salt leaching method adapted from previous literature.^[5] Briefly, sieved sodium chloride (NaCl, salt) crystals (250-425 μm, 65 wt% to the total weight of salt, dry polymer and HA) were added to desired amounts of HA, THA or AgTHA and POC prepolymer solution (30 wt% in 1,4-dioxane) then stirred to evaporate the solvent until the mixture became a viscous solid. The scaffolds were dried in cuboid Teflon molds and cut into 10 × 10 × 20 mm dimensions and crosslinked at 80 °C for 3 days then 120 °C under vacuum for another day. After crosslinking, salt was leached from the scaffolds in DI water followed by lyophilization and sterilization.

Lumbar fusion surgery

Healthy New Zealand rabbits (n = 40; 2-2.5 kg) purchased from the Laboratory Animal Center of Southern Medical University (Guangzhou, China) were randomly divided into 5 groups (8 rabbits per group): POC-HA (material control), POC-HA/THA, POC-THA/AgTHA, autograft bone (AB, positive control), and no treatment (negative control). All animal experiments were carried out in compliance with the protocol approved by Southern Medical University's Animal Care and Use Committee (Guangzhou, China).

Before the surgery, all animals were fasted for eight hours. All surgical tools were autoclaved before use. The rabbits were anesthetized by the injection of 2% pentobarbital sodium (30 mg/kg) via the marginal ear vein. The surgery area on the back of rabbit was sterilized once the 4th (L4) and 5th (L5) lumbar vertebral bodies on the back of rabbit were localized. A 6-8 cm length incision along the L4 and L5 lumbar spinous processes was created. The skin and the subcutaneous tissue were cut through to expose the left and right lamina. The paraspinal muscles beneath the periosteum were peeled away to expose the articular process. The spinal process was broken and removed by a three-joint rongeur. The cortical bone of the L4 lumbar plate was shaped by a grinding brick to create a 20 × 10 mm defect along the spinous process serving as the midline. The composite scaffold or autograft bone was embedded into the defect. For the blank control group, the defect was kept empty with no implantation. A steel plate was fixed on the L4 and L5 lumbar superior articular processes using two steel screws to prevent movement of the implanted material and provide mechanical support during the animal study process. Finally, the muscles, fascia and skin incisions were sutured.

Post-surgery study

For each test or control group, 4 randomly selected rabbits were sacrificed with CO₂ at 8 and 12 weeks, respectively. The bone tissue sections including the implanted material were harvested for post-surgical analyses including visible observation, micro-computer

tomography (micro-CT) and histological examination to assess the *in vivo* biocompatibility and bone regenerative performance of the tested composite scaffolds.

The harvested bone sections were fixed in 4% paraformaldehyde solution for one week before visible observation and the micro-CT analyses. The micro-CT scanning and analysis was conducted using a micro-CT imaging instrument (Aloka Latheta LCT-200, Hitachi-Aloka Medical, Ltd., Japan) in The Third Affiliated Hospital of Southern Medical University (Guangzhou, China). An isolated bone model (pixel size: 240 μm ; slice thickness: 240 μm ; speed: integ. 2; rotation angle: 360°; X-ray voltage: low; artifact removal: lean; sync. scan: no; metal artifact reduction: no) was used to scan the entire L4 lamina area. Three-dimensional (3D) and two-dimensional (2D) images were reconstructed with VGStudio MAX 2.2.2 software. A quantitative 3D histomorphometric evaluation was then performed on a rectangular volume of interest (VOI) using an established method to determine the bone mineral density (BMD).^[6]

Histological examination began at preset time points (8 and 12 weeks post-operation). After being fixed in 4% paraformaldehyde for 1 week, the harvested bone sections were soaked in ethylenediaminetetraacetic acid (EDTA) solution for 30-60 days. The fluid was replaced every day until the calcium was completely removed followed by paraffin embedding. The decalcified tissue paraffin sections (thickness = 4 μm) sectioned by a SP2500 microtome (Leica Microsystems, Germany) were then stained by hematoxylin and eosin (H&E), Masson's trichrome, Safranin O/Fast green and immunohistochemical (for OCN, osteocalcin) staining methods following standard protocols provided by the manufacturer. The stained sections were then photographed and analyzed under an Olympus BX51 microscope (Center Valley, PA, USA).

Statistical analysis

Data were analyzed using SPSS statistics 20 statistical software (SPSS, Inc., Chicago, IL, USA). All quantitative results are expressed as mean \pm standard deviation. The statistical

significance between two sets of data was determined by one-way analysis of variance (ANOVA). Data were taken to be significant if $p < 0.05$ (*) was obtained.

References

- [1] J. Yang, A. R. Webb, G. Ameer, *Adv. Mater.* **2004**, *16*, 511.
 [2] J. Yang, A. R. Webb, S. J. Pickerill, G. Hageman, G. A. Ameer, *Biomaterials* **2006**, *27*, 1889.
 [3] J. Guo, Z. Xie, R. T. Tran, D. Xie, D. Jin, X. Bai, J. Yang, *Adv. Mater.* **2014**, *26*, 1906.
 [4] A. Oyane, H.-M. Kim, T. Furuya, T. Kokubo, T. Miyazaki, T. Nakamura, *J. Biomed. Mater. Res., A*, **2003**, *65*, 188.
 [5] J. Tang, J. Guo, Z. Li, C. Yang, D. Xie, J. Chen, S. Li, S. Li, G. B. Kim, X. Bai, Z. Zhang, J. Yang, *J. Mater. Chem. B* **2015**, *3*, 5569.
 [6] I. Kallai, O. Mizrahi, W. Tawackoli, Z. Gazit, G. Pelled, D. Gazit, *Nat. Protoc.* **2011**, *6*, 105.

Table S1. Elemental compositions of HA, THA and AgTHA determined by EDS.

Sample	Elements (wt%)				
	C	O	Ca	P	Ag
HA	0	45.56	35.28	19.16	0
THA	6.75	42.70	33.27	17.64	0
AgTHA	3.65	41.25	32.61	17.11	1.73

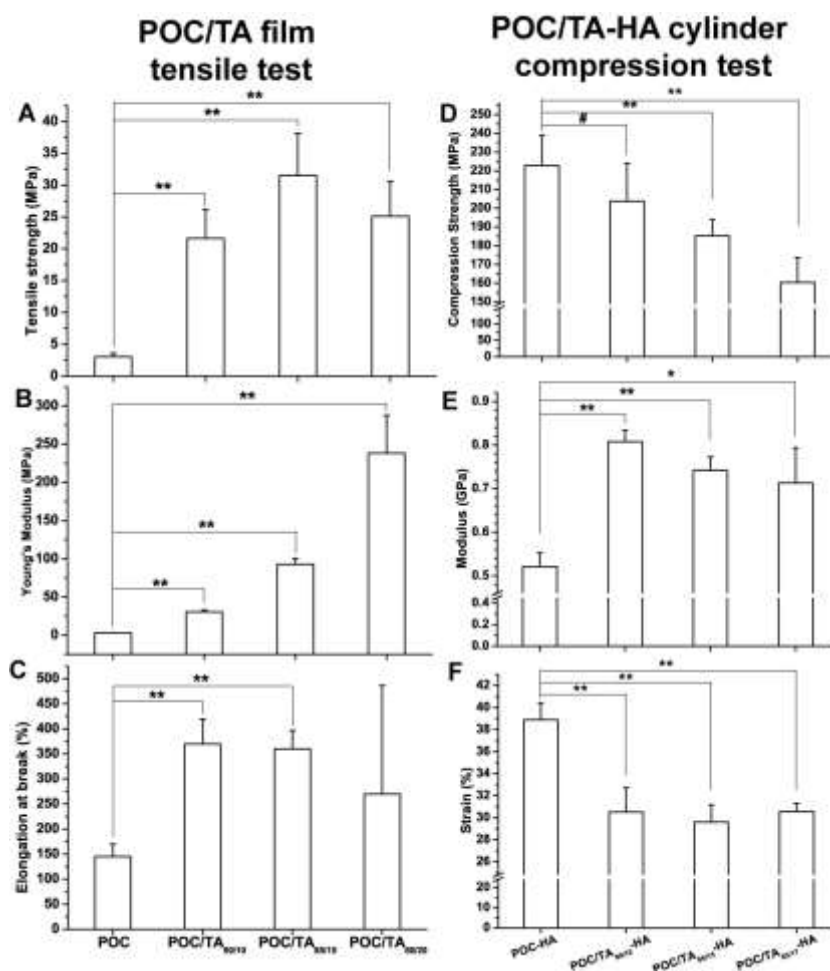


Figure S1. The tensile test results of POC and POC/TA (w/w = 90/10, 85/15, 80/20) films (crosslinking condition: 100 °C, 3 days) (A: tensile strength, B: Young's modulus, C: elongation at break) and the compression test results of POC-HA (60 wt% HA) and POC/TA(w/w = 90/10, 85/15 or 83/17)-HA (60 wt% HA) composite cylinders (Crosslinking condition: 80 °C, 3 days plus 120 °C, vacuum, 1 day) (D: compression strength, E: modulus, F: strain). # $p > 0.05$, * $p < 0.05$, ** $p < 0.01$.

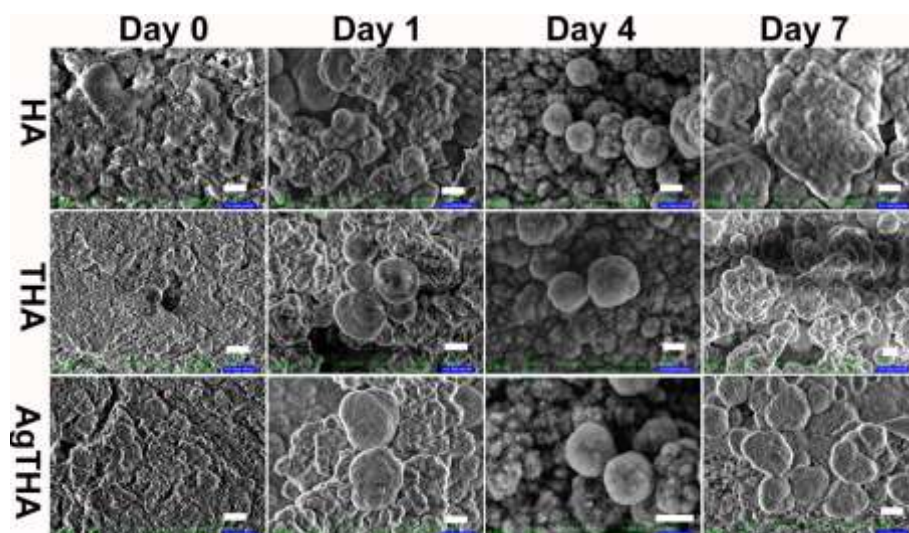


Figure S2. SEM images of mineral deposition on HA-, THA- and AgTHA-coated silicon wafers before and after being incubated in 5 times concentrated simulated body fluid (SBF-5 \times) for 1, 4 and 7 days. The scale bar is 2 μ m.

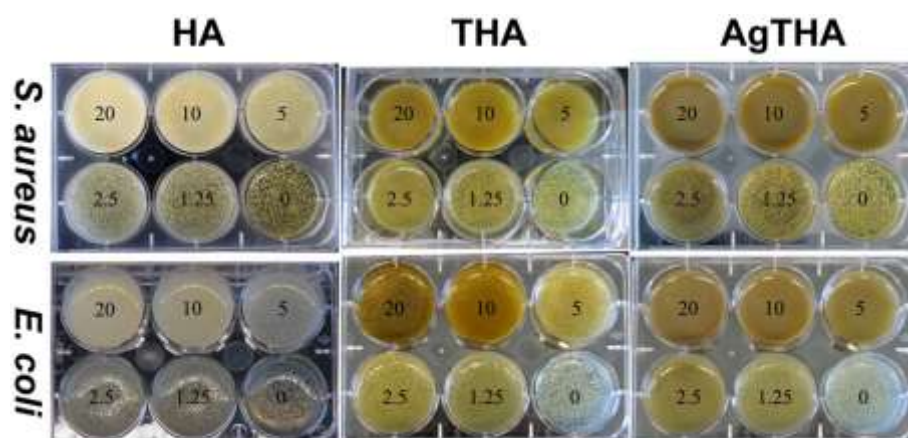


Figure S3. Photographs of bacterial growth on agar plates containing different concentrations (numbers shown in the wells, mg/mL) of HA, THA and AgTHA particles for minimum inhibition concentration (MIC) tests against *S. aureus* and *E. coli*.

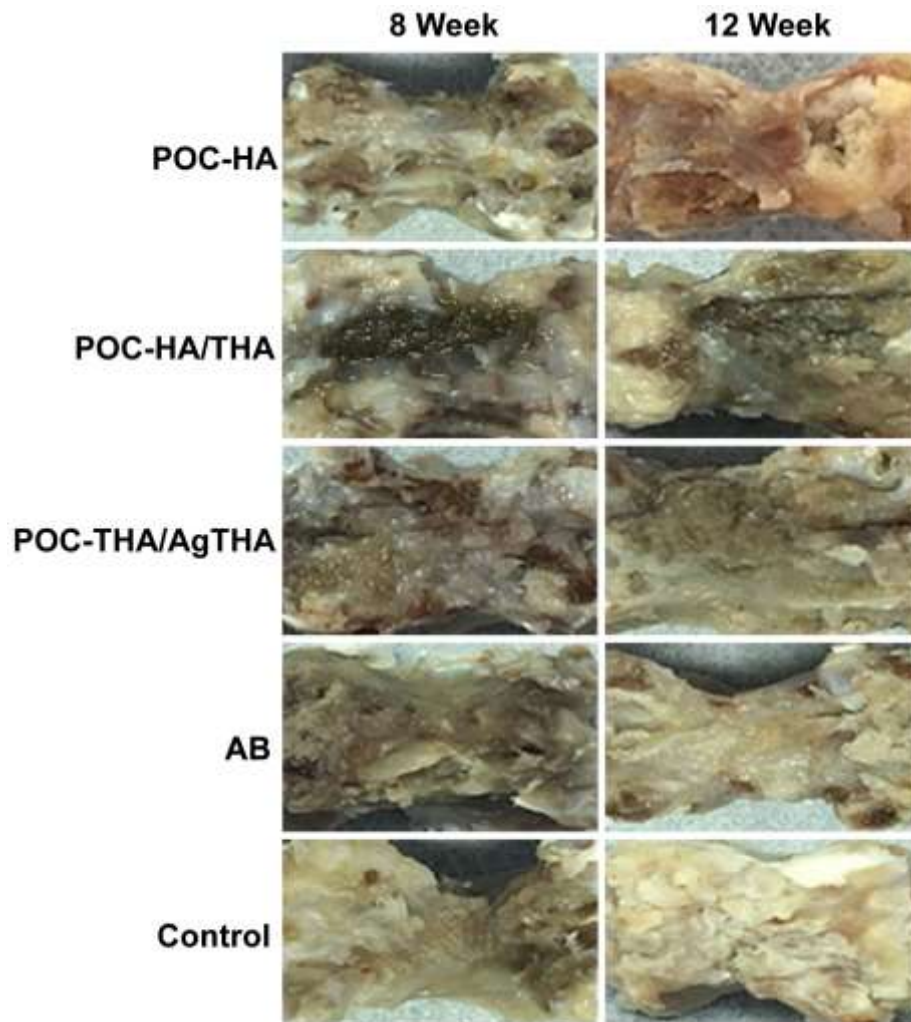


Figure S4. Photos of harvested bone tissue sections of the treatment and control groups at week 8 and week 12 post lumbar fusion surgery. (AB: autograft bone; Control: empty defect.)

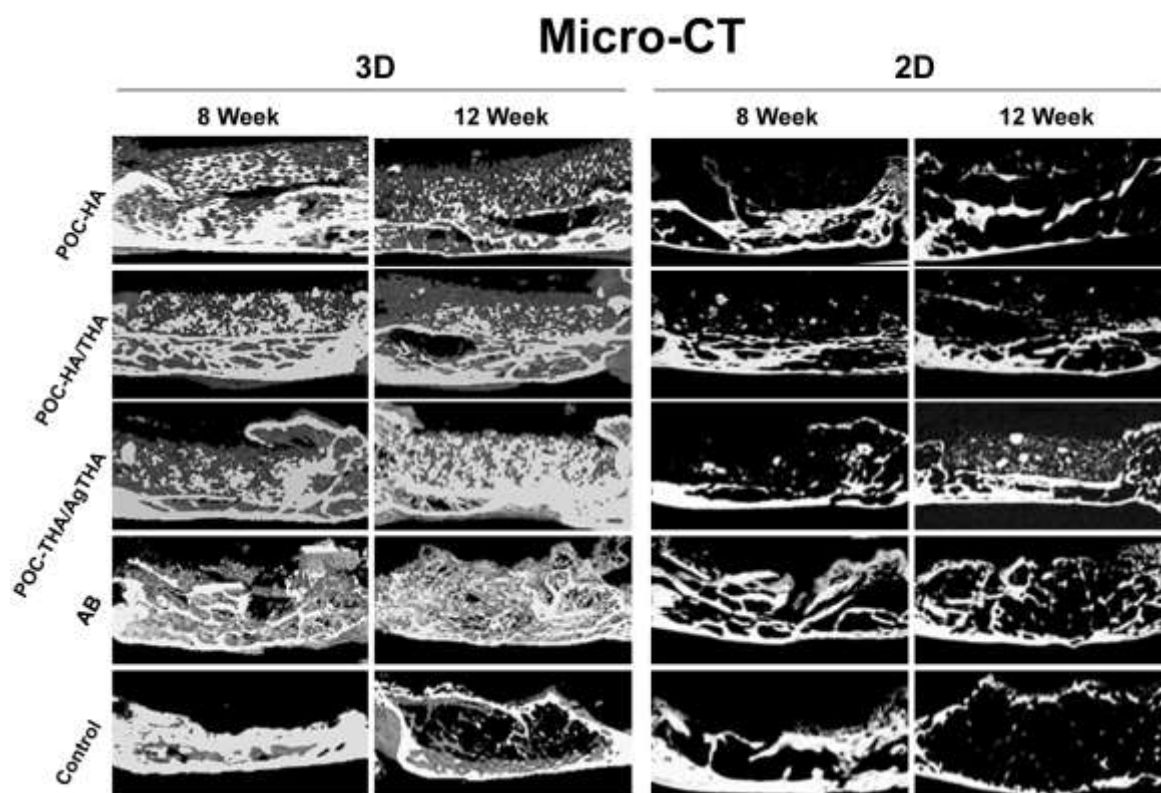


Figure S5. The three-dimensional (3D) and two-dimensional (2D) reconstruction images obtained by micro-computer tomography (micro-CT) of harvested bone sections of different samples at week 8 and 12. (AB: autograft bone; Control: empty defect.)